

Cretaceous and late Cenozoic uplift of the eastern French Massif Central: insights from low- temperature thermochronometry

Valerio Olivetti, Maria Balestrieri, Vincent Godard, Olivier Bellier, Cécile Gautheron, Pierre P.G. Valla, M. Zattin, Faccenna Claudio, Rosella Pinna Jamme, Kevin Manchuel

▶ **To cite this version:**

Valerio Olivetti, Maria Balestrieri, Vincent Godard, Olivier Bellier, Cécile Gautheron, et al.. Cretaceous and late Cenozoic uplift of the eastern French Massif Central: insights from low- temperature thermochronometry. Lithosphere, 2020, 12 ((1)), pp.133-149. 10.1130/L1142.1 . hal-02464552

HAL Id: hal-02464552
https://hal.science/hal-02464552

Submitted on 3 Feb 2020

HAL is a multi-disciplinary open access archive for the deposit and dissemination of scientific research documents, whether they are published or not. The documents may come from teaching and research institutions in France or abroad, or from public or private research centers.

L'archive ouverte pluridisciplinaire **HAL**, est destinée au dépôt et à la diffusion de documents scientifiques de niveau recherche, publiés ou non, émanant des établissements d'enseignement et de recherche français ou étrangers, des laboratoires publics ou privés.

Lithosphere
E: lithosphere@geosociety.org
W: geosociety.org/gsa
T: @geosociety

FOR PEER REVIEW - CONFIDENTIAL

Cretaceous and late Cenozoic uplift of the eastern French Massif Central: insights from low-temperature thermochronometry

Tracking no:

Authors:
Valerio olivetti (university of Padova), Maria Balestrieri, Vincent Godard (Aix-Marseille University), Olivier Bellier (Aix-Marseille University), Cecile Gautheron (UniverSud Paris), Pierre Valla (University of Grenoble Alpes, University of Savoie Mont Blanc), Massimiliano Zattin (University of Padova), Claudio Faccenna (Università Roma TRE), Rosella Pinna-Jamme (GEOPS, Univ. Paris-Sud, CNRS, Université Paris-Saclay), and Kevin Manchuel (EDF)

Abstract:
Apatite fission-track and (U-Th)/He thermochronometry have been applied to investigate the long-term topographic evolution of the French Massif Central. Located in the foreland domain of the Alpine and Pyrenean mountain belts, the French Massif Central presents enigmatic topographic features, reaching ~1700 m a.s.l. and ~1000 m of relief, that did not originate from Alpine compressional nor from extensional tectonics. The age of the present-day topography, the timing of its formation, and the underlying processes remain debated. Our new thermochronological data come from the eastern flank of the massif, where sampling profiles run from the high-elevation region down to the Rhône river valley floor with a total elevation profile of 1200 m. Age-elevation relationships, mean track-length distributions and thermal modeling indicate a two-steps cooling history: (i) a first exhumation event, already detected through previously-published thermochronology data, with an onset time during Mid-Cretaceous; and interestingly (ii) a more recent Cenozoic phase that is resolved from our data, with a likely post-Eocene onset. This second erosional event is associated with relief formation and valley incision probably induced by a long wavelength domal uplift supported by mantle upwelling.

Disclaimer: This is a confidential document and must not be discussed with others, forward in any form, or posted on websites without the express written consent of the Geological Society of America.

Cretaceous and late Cenozoic uplift of the eastern French Massif Central: insights from low-temperature thermochronometry

Valerio Olivetti[1,2], Maria Laura Balestrieri[3], Vincent Godard[1], Olivier Bellier[1], Cécile Gautheron[4], Pierre G. Valla[5,6], Massimiliano Zattin[2], Claudio Faccenna[7], Rosella Pinna Jamme[4], Kevin Manchuel[8].

1 Aix Marseille Univ, CNRS, IRD, INRA, Coll France, CEREGE, Aix-en-Provence, France

2 Dipartimento di Geoscienze, Università di Padova, Italy.

3 CNR, Istituto di Geoscienze e Georisorse, Firenze, Italy.

4 GEOPS, Université Paris-Sud, CNRS, Université Paris-Saclay, 91405 Orsay, France.

5 Univ. Grenoble Alpes, Univ. Savoie Mont Blanc, CNRS, IRD, IFSTTAR, ISTerre, 38000 Grenoble, France.

6 Institute of Geological Sciences and Oeschger Center for Climate Research, University of Bern, Bern, Switzerland.

7 Dipartimento di Scienze, Università di Roma Tre, Italy.

8 EDF-DIPNN-DI-TEGG, Aix en Provence, Cedex 02, France.

ABSTRACT

Apatite fission-track and (U-Th)/He thermochronometry have been applied to investigate the long-term topographic evolution of the French Massif Central. Located in the foreland domain of the Alpine and Pyrenean mountain belts, the French Massif Central presents enigmatic topographic features, reaching ~1700 m a.s.l. and ~1000 m of relief, that did not originate from Alpine compressional nor from extensional tectonics. The age of the present-day topography, the timing of its formation, and the underlying processes remain debated. Our new thermochronological data come

from the eastern flank of the massif, where sampling profiles run from the high-elevation region down to the Rhône river valley floor with a total elevation profile of 1200 m. Age-elevation relationships, mean track-length distributions and thermal modeling indicate a two-steps cooling history: (i) a first exhumation event, already detected through previously-published thermochronology data, with an onset time during Mid-Cretaceous; and interestingly (ii) a more recent Cenozoic phase that is resolved from our data, with a likely post-Eocene onset. This second erosional event is associated with relief formation and valley incision probably induced by a long wavelength domal uplift supported by mantle upwelling.

1. INTRODUCTION

Many mountain belts on Earth are not associated with convergent domains and crustal shortening. These kind of intraplate, uncommon orogens are characterized by low seismic activity, slow deformation rate and by a typical long wavelength geomorphological pattern with slowly-eroding high-elevated plateaus and erosion mainly focused along their margins (e.g. Stanley et al., 2013; Scotti et al., 2014). The Massif Central in France is a striking example of such a non-convergent mountain; it is located away from the European-African plate boundary and was not involved in its Cenozoic convergence. It is nowadays a prominent topographic feature reaching up to 1700 m a.s.l. (Fig. 1) with a low-relief and high-elevation landscape bordered by incised fluvial valley (up to 1000 m of relief) (Fig. 1b and 1c), but the processes responsible for the creation and persistence of this relief have not been clearly elucidated yet.

Insights on the geodynamics of the Massif Central may come from the reconstruction of the timing, rates and amount of the relief growth. Different scenarios can be postulated for the origin of its topography, spanning from (1) a long-lasting persistence of a Hercynian range underwent to a slow erosion-induced isostatic uplift or (2) a recent topographic rejuvenation hypothesis, which is supported by many geomorphological evidences, such as recent river incision, a non-monotonic

uplift, multiple levels of perched surfaces (Seranne et al., 2001; Olivetti et al., 2016) as well as a complex history of burial and exhumation phases highlighted by thermochronology (Barbarand et al., 2001; Peyaud et al., 2005; Gautheron et al., 2009). In the framework of this rejuvenated topography hypothesis, the age and mechanism for the regional uplift are yet not explicitly defined and could encompass different phases such as a post-Miocene uplift event induced by the Messinian salinity crisis (Clauzon 1982), a Miocene uplift phase triggered by mantle upwelling or an Oligocene event associated to rifting and opening of the Liguro-Provencal Basin (Seranne et al., 2001; Faccenna et al., 2010) (Fig. 1a).

The actual timing and mechanism for the formation of the topography of the Massif Central, thus, is still unclear but the general current interpretation implies a contribution of a mantle upwelling leading in turn to volcanic activity that deeply shaped the landscape of the massif since the Miocene (i.e. Michon and Merle, 2001). Numerous geophysical campaigns were carried out in the nineties that highlighted a seismic low velocity zone 300 to 150 km deep, high heat flux and negative Bouguer gravity anomaly (Granet et al., 1995; Sobolev et al., 1997). All these observations are consistent with the interpretation of a shallow mantle and thus potential mantle contribution to the late-stage topographic evolution of the Massif Central.

Although several studies have reported evidence for river incision throughout the massif (see Seranne et al., 2001 for instance), an attempt to reconstruct a large-scale and long-term topography evolution of the massif is lacking. To address this topic, we performed a new thermochronological study based on apatite (U-Th)/He and fission-track analysis and implemented them with literature data (Barbarand et al., 2001; Gautheron et al., 2009). Sampling has been performed along the eastern margin of the Massif Central, from the high-elevation surfaces to the bottom of the Rhône valley, in order to cover the entire margin profile (total elevation transect of 1200 m). The eastern margin of the massif should have recorded the signal of the erosion induced by the uplift of the entire massif

because the long persistence of the Rhône river formed a stable regional base level for erosion processes.

2. GEOLOGICAL SETTING

2.1 Tectonic history

The French Massif Central is mainly composed by rocks associated with the Hercynian orogeny (Devonian to Late Carboniferous), dominated by granites and high-grade metamorphic rocks with subordinate mafic and ultramafic rocks and Late Paleozoic sedimentary covers (Chantraine et al., 2003) (Fig. 2a). Paleozoic rocks are overlain by thin Triassic continental sandstones and by Triassic to Cretaceous mainly carbonate sediments that characterize the sedimentation of the entire northern margin of the Tethys basin. During late Cretaceous, the Pyrenean orogeny involved mainly the southern portion of the massif, and reactivated Paleozoic structures with mainly strike slip kinematics (Blès et al., 1989).

The Oligocene rifting event, recognized in the whole Western and Central Europe, involved mainly the northern and eastern part of the massif, producing north-south elongated basins marked by several hundreds of meters, locally up to 1-2 km, of marine to lacustrine sediments (Limagne, Roanne, Bresse and Valence basins) (Fig. 2a-b). Along the southern margin of the Massif, the European Oligocene rifting event overlapped with the opening of the Gulf of Lion that induced extensional tectonics along reactivated Paleozoic features such as the Nimes and Cévennes faults (Fig. 2a-b).

The long-lasting volcanic history of the Central Massif starts back to the early Cenozoic and it evolved in three stages (Michon and Merle 2001 and references therein): (i) a pre-rift Paleocene phase, with limited magmatic production, (ii) a rift-related phase found in the northern part of the massif only and (iii) the main phase from ~27 Ma to the Quaternary. During this last phase, the major magmatic activity occurred from middle Miocene (~15 Ma) to the Quaternary with a climax between

9 and 6 Ma when the volume of erupted magma was much larger than during any other magmatic event in this area. The erupted magmas are sub-alkaline to alkaline intraplate-type lavas (Lustrino and Wilson, 2007).

Alpine orogeny only marginally affected the Massif Central and although the Alpine frontal thrusts are nowadays only a few tens of kilometers to the east, no evidence of Alpine deformation is reported within the crystalline basement of the massif (Blés et al., 1989).

2.2 Long-term history of vertical movements in the Massif Central

The early Triassic topography of the Massif, at the end of the Hercynian orogenic cycle, is supposed to be characterized by low elevations, limited relief and marginal plains (Le Griel, 1988) bordered by marine basins that hosted carbonate sedimentation (Curnelle and Dubois, 1986). Hercynian basement should have been close to the base level during the whole Jurassic, without evidence of a prominent topography capable to produce large fluvial system and clastic sediments (Le Griel, 1988). Contrastingly, an important phase of surface uplift and consequent crustal exhumation occurred during the Cretaceous, based on low temperature thermochronological data (Barbarand et al., 2001; Peyaud et al., 2005; Gautheron et al., 2009) and stratigraphic constraints (Curnelle and Dubois, 1986). This mid-Cretaceous exhumation is coeval with opening of the Bay of Biscay and slightly predates the emersion of the "Ithsme Durancien", an aerially exposed E-W elongated area emerged during the Cenomanian that led to the formation of large bauxite deposits. Emersion of the "Ithsme Durancien" is associated to a NE-SW directed extensional tectonic regime, that produced the formation of the Vocontian Basin to the north and South Provence Basin to the south (Tavani et al., 2018 and references therein). During lower Cretaceous, topography of the southern Massif Central should have been characterized by long wavelength of ~500 km and moderate amplitude 300-500 m (Wyns and Guillocheau, 1999) produced by far field response to the Pyrenean orogeny. Cretaceous low topography is suggested also by the limited clastic sedimentation

125 within the subsiding marine basins, such as the Grand Causse, coeval with the exhumation of the
126 Cévennes and Ardèche regions (Barbarand et al., 2001; Gautheron et al., 2009).

127 During the Paleocene, large portions of the south-eastern massif, located south of the Cévennes
128 Fault, were emerged as a consequence of the Pyrenean compression, while there are no significant
129 evidence of Pyrenean activity farther north, and the topography should have been limited to few
130 hundred meters high (Séranne et al., 2002 and references therein).

131 Numerous stratigraphic evidences suggest that during the lower Eocene a large portion of the
132 Massif Central was close to sea level. Marine clays and evaporitic deposits are described in the Velay
133 region, in the central part of the massif (Girod et al., 1979; Rey, 1971; Turland, et al., 1994), while
134 the sedimentation in the Bresse basin recorded a marine communication with the Valence basin and
135 the Mediterranean Sea (Sissingh, 1998). In the southern part of the massif, marine deposits are
136 described in the Ales basin (Alabouvette and Cavelier, 1984).

137 The Oligocene rifting produced deep grabens mainly in the northern massif, that hosted up to
138 two-three thousand meters of sediments (Limagne basin), characterized by lacustrine-continental
139 facies with regular marine incursions. Oligocene rifting induced medium to high crustal thinning
140 (between 5 and 25%) but not associated to a large emission of volcanic products (Michon and Merle,
141 2001). The lack of Oligocene thermochronological cooling age also suggests that there were no
142 significant exhumation event (Fig. 2c; Barbarand et al., 2001; Peyaud et al., 2005; Gautheron et al.,
143 2009).

144 In the center of the massif (Margeride and Velay regions), geometric relationship between river
145 incision and volcanic flows allowed to constrain multiple river incision events between 10 Ma and 7
146 Ma attesting an uplift phase of the order of 200-300 m (Michon, 2000 and references therein; Goër
147 and Etienne, 1991; Augendre, 1997; Defive and Cantagrel, 1998) while in the Causse region
148 (southern massif) the incision of the Tarn river was active already at 13 Ma (Ambert, 1994). In
149 general, the Miocene to present incision history of the most of the Massif Central area is focused in a

10 to 5 Ma minor phase (13 to 7) followed by a major phase of river incision, evaluated at around 400 m, suggesting an important and coeval uplift event (Etienne, 1970; Defive and Cantagrel, 1998; Michon, 2000; Séranne et al., 2002). This second phase of uplift has been recently detected by river profile analysis and cosmogenic nuclides derived denudation rates along the eastern margin of the massif, and has been consistently evaluated to be of the order of 300 to 400 m (Olivetti et al., 2016).

2.3 Thermochronological data

Previous thermochronological studies focused along the south and south-eastern portions of the Massif Central (Fig. 2c). The Ardèche and Cévennes areas, where the relief is greater, have been investigated through apatite fission track (AFT) by Barbarand et al. (2001) and through (U-Th)/He (AHe) method performed on the same samples by Gautheron et al. (2009). The positive correlation between age and elevation both for AHe and AFT data has been interpreted as a consequence of long-lasting exhumation since 130 Ma (apparent exhumation rate of between 0.013 and 0.022 km/Myr), leading to slow cooling through the apatite Partial Annealing Zone (PAZ) and the He Partial Retention Zone (PRZ).

Samples from Cévennes and Ardèche regions yielded AFT and AHe ages spanning between ~130 Ma to 45 Ma, and thermal modeling suggests an exhumation event started at about 130±10 Ma (Barbarand et al., 2001). A very similar thermal history is proposed by Peyaud et al. (2005) using AFT ages (spanning between 147 Ma and 77 Ma) and vitrinite reflectance data for the region of the Rouergue and Montagne Noire (Fig. 2c). Apart from this well-defined pre-Cenozoic thermal histories, in the Cévennes mountains (Saint Guiral Liron profile) Barbarand et al. (2001) observed a characteristic shape of the mean track length (MTL) vs AFT age relationship, where the youngest and oldest ages display relatively long mean track lengths while the intermediate ages have shorter track lengths. Such a relationship ("boomerang" shape) is likely the consequence of a period of thermal annealing, affecting a set of samples to various degrees, followed by a discrete cooling event

(Green, 1986; Omar et al., 1989). The oldest ages represent shallower, cooler rocks preserving most of their tracks and previous thermal histories, while intermediate ages (the middle "concave-up" section) represent rocks that resided a long time within the PAZ whose tracks were more severely shortened. The timing of the cooling event is recorded by "deepest" youngest samples provided that they have MTLs of the order of 14 µm (i.e. they were at paleotemperatures > c. 110°–125°C prior to the last phase of cooling), otherwise they provide just an upper limit to this timing. In the dataset of Barbarand et al. (2001), the younger part of the "boomerang" pattern is less well defined and the youngest sample display an age of 45±2 Ma accompanied by a MTL of 12.9±0.2 µm. Additional data are thus required to further elucidate the recent exhumation history of the Massif and its relationship with topographic evolution mechanisms.

3. METHODS

In a context of ancient, slowly-eroding orogen, thermochronological methods with low-closure temperatures assure greater probability to detect any recent topographic rejuvenation. For that purpose, we mainly used apatite (U-Th)/He dating for its low closure temperature (40-120 °C; Gautheron et al., 2009; Flowers et al., 2009; Djimbi et al., 2015) complemented by some AFT data (closure temperature of 110 °± 10° C; Green and Duddy, 1989) for a subset of samples to expand the time window of investigation. Samples have been collected following tens of km long profiles along the eastern flank of the massif with as large as possible differences in elevation, from the low-relief high-elevation surface down to the bottom of the Rhône valley following the classical sampling strategy used for plateau margin studies (i.e. Persano et al., 2001). Analytical protocols for apatite (U-Th)/He and AFT analysis adopted in this study follows Mahéo et al. (2013) and Balestrieri et al. (2001), respectively, and the corresponding procedures are presented in the appendix.

Rock cooling history has been investigated by inverse and forward numerical modeling using QTQt and Hefty software (Gallagher, 2012; Ketcham, 2005). QTQt software has been used for

inverse modeling, where observed AFT and AHe data such as spontaneous, induced and horizontal confined tracks, apatite crystal dimension, amount of Uranium, Thorium and measured age, are inverted to find the Temperature-time (T-t) paths compatible with the data. Hefty software has been used in forward method, where a T-t path is proposed following some specific topographic/exhumation scenarios and the synthetic AFT age and track length distribution are produced and then compared to observed data.

The Ketcham et al. (2007) annealing model and the radiation damage accumulation and annealing model of Gautheron et al. (2009) have been applied for AFT and AHe data, respectively.

4. RESULTS

4.1 Thermochronological data

Twelve bedrock samples of granite and high-grade metamorphic rocks have been collected along the eastern side of the Massif Central (Fig. 3). Single-crystal apatite (U-Th)/He dating (afterward referred to AHe) was performed on all samples and where possible five replicates were performed (Table 1). Some replicates present older ages in comparison to others inside the same samples, reflecting variable grain size, damage content created during alpha decay, chemical composition, and complex diffusion processes (Shuster et al., 2006; Flowers et al., 2009; Gautheron et al., 2009; Gautheron et al., 2013; Recanati et al., 2017). AFT dating and track-length measurements were performed on 5 samples (Table 2). In general, the ages show a positive correlation with elevation (Fig. 3), and the regression of the age-elevation yields an apparent exhumation rate of 0.038 km/Myr.

The northern profile is composed of 4 samples collected from elevation between 471 m and 1366 m asl, along the southern flank of the St. Etienne valley. The valley is around 25-km wide and the horizontal distance of our sampling profile is 12 km for a total elevation difference of 700 m (Fig. 3). Single-grain AHe ages span from 58 to 131 Ma. 5 grains have been dated for the lower three

samples, while the uppermost sample yields only a single-grain age of 131 Ma. Two AFT ages from the highest and lowermost samples show ages of 93±4 Ma (vo-14, 1136 m asl) with a long MTL of 13.9±0.1 µm (100 measured tracks) and 78±5 Ma (vo-16, 471 m asl) with a MTL of value of 12.7±0.2 µm (51 measured tracks), respectively.

The southern profile is composed of 7 samples from an elevation of 195 m to 922 m, along a horizontal distance of about 40 km starting from the low-relief upland surface to the Rhône river and for a total difference in elevation of about 900 m. Single-grain AHe ages span from 40 to 134 Ma. The three lowermost samples (vo-1, vo-2, vo-3) have similar single-grain AHe ages with many young ages (between 94 and 40 Ma) consistently with their low elevations. Two samples at 350 m (vo-4) and 220 m (vo-3) of elevation, respectively, have been dated by AFT and yielded ages of 80±4 Ma with MTL of 12.9±0.2 µm (100 measured tracks) and 68±4 Ma accompanied by an MTL of 13.3±0.2 µm (100 measured tracks).

Three samples have been collected along a transect in between the two profiles (vo-18, vo-19, vo-21) with single-grain AHe ages spanning between 40 and 129 Ma. Sample vo-21 is the lowermost sample collected in this study and shows a high dispersion in single-grain AHe ages, nevertheless two replicates have young ages of 40 Ma and 50 Ma. The corresponding AFT age is 74±4 Ma with MTL of 13.3±0.1 µm (100 measured tracks).

4.2 Thermal modeling

The spread of the AHe ages reflects the effective Uranium content (eU, defined as U + 0.235 × Th), the grain size (sphere equivalent radius Rs) and the thermal history (e.g. Gautheron et al., 2009). eU content is highly variable between the apatite crystals (Table 1) but within the same sample it is often positively correlated with the ages suggesting an important control on age dispersion by radiation damage effect (Fig. S1). This age tendency is similar to what obtained by Gautheron et al. (2009) for samples collected some tens of km southward: the age overlap between the two AFT and

AHe thermochronometers is proposed to reflect the level of radiation damage and the thermal history. In case of reheating or long stay in the He partial retention zone (PRZ), a high level of α-recoil damage can remarkably move the He PRZ towards higher temperatures ranging up to 120 °C, making the closure temperature for the AHe system close to that one of the AFT system (Gautheron et al., 2009).

To evaluate the thermal evolution of individual samples, taking into account both the influence of the α-recoil damage and grain size for the AHe system and AFT data, we performed 1D thermal modeling using the QTQt software (Gallagher, 2012). Figure 4 shows the results of the modeling for the southern profile, using AFT ages plus MTLs and AHe ages with radiation damage model for He diffusion (Gautheron et al., 2009) with the timing of the Cretaceous limestones as the only external stratigraphic constraint.

Thermal history of vo-14 (the uppermost sample) has been modeled in three different ways, in order to evaluate the role of He data and stratigraphic constraint on the inverse modeling: with He data (Fig. 4a), without He data (Fig. 4b) and without stratigraphic constraint (red lines in Fig. 4b). Thermal histories with He data are remarkable similar than those without He data (probably due also to limited number of AHe-dated grains), suggesting that general modeling path are mainly controlled by the AFT ages and MTL while the He data contribute to better define the paths. For this sample, the Mesozoic stratigraphic constraint does not modify the post-100 Ma thermal histories, suggesting that a Mesozoic burial under the Triassic and Jurassic sediments is not constrained by thermochronological data for the uppermost sample.

For the low-elevation samples the general thermal history shows a similar trend, with a faster cooling phase from 120-100 Ma and 70-50 Ma followed by a less well-defined evolution suggesting a slow cooling and a long persistence around 50-40 °C until present-day.

It is noteworthy that the He data for the lowermost samples (vo-3 and vo-21, Figs. 2d,e) substantially constrain the thermal history, that resulting consistent between each other. The highly-

dispersed He data of the vo-4 sample (ranging from 89 Ma to 65 Ma), prevent their use in the modeling and the Cenozoic T-t path cannot be precisely defined (Fig. 2f).

5. DISCUSSION

5.1 Regional distribution of the thermochronological ages

The episodes that shaped the topography of the Massif Central are unclear because of the limited available time constraints for tectonic deformation events and geomorphological markers. The margin of the massif records a long morphogenesis history (see Seranne et al. 2001 and references therein), evolving under general slow erosion rates confirmed also by our new thermochronological data preserving the record of the Cretaceous exhumation and a probable evidence of Cenozoic imprinting (discussed below). In order to trace the feeble tectonic signal in the thermochronological data, here we compare our data set to the published data of Barbarand et al. (2001) and Gautheron et al. (2009). In particular, we found three common characteristics that we consider diagnostic for the reconstruction of the tectonic history: i) uppermost samples show AFT and AHe Cretaceous ages and long MTLs; ii) non-monotonic trend of the MTL with age and elevation, showing a general decrease from high elevation/old age toward intermediate elevations and eventually a slightly increase for the lowermost and youngest samples (Fig. 5); iii) large differences in AHe and AFT ages for a limited difference in elevation between the uppermost and lowermost samples.

The AFT age and MTL of our uppermost sample (vo-14; 93±8 Ma and MTL of 13.9 μm), located at 1136 m asl, are consistent with samples n°20 (105±6 Ma, MTL of 13.76 μm at 1500 m) from Cévennes and with sample n°8 (119±4 Ma, MTL of 13.71μm at 1185 m) from Ardèche regions reported in Barbarand et al. (2001). Also the single-grain AHe ages of our vo-14 and n°20 Cévennes samples overlap, being between 88 and 120 Ma. These ages confirm the proposed interpretation of Barbarand et al. (2001) and Peyaud et al. (2005) about a relatively fast and widely diffuse Cretaceous

300 erosion phase probably induced by the regional uplift associated with the Pyrenean Rifting event.
301 Initiation of this phase could have been around 120±10 Ma as derived by the thermal modeling of our
302 data, which is consistent with Barbarand et al. (2001). The observed regional variations could reflect
303 along margin changes in tectonic evolution which will be discussed below.

304 The relationship of MTL with elevation and ages is similar in all the three regions of Cévennes,
305 Ardèche and our study area (called NE margin); the MTLs tend to decrease from the high elevation
306 to about 600-400 m, then they tend to slightly increase from 400 m to the bottom of the profile (Fig.
307 5). This trend is highlighted by the 2nd order polynomial regression curves (calculate with age vs
308 elevation transposed in horizontal and then vertically rotated). The same trend is observed in the
309 MTL vs AFT ages (Fig. 5d) where the age pattern assumes a typical concave-up "boomerang" shape
310 that is classical observed in the passive continental margins (Green 1986; Gallagher and Brown
311 1999). Although the overall geodynamics evolution of the eastern Central Massif is very different
312 from a continental margin, we remark the similarity in term of erosional style that could reflect
313 comparable tectonic and geomorphological evolutions.

314 In the classical interpretation of these boomerang shapes for continental margins (Gallagher
315 and Brown 1999; Wildman et al., 2018), the upper samples preserve the erosional history of the pre-
316 modern margin formation, in our case the Cretaceous Pyrenean rifting (blue area in Fig. 5a, b, c),
317 while the lower samples record the evolution of the modern escarpment. In our case, the ages of the
318 low-altitude samples do not precisely constrain the onset of margin erosion, because exhumation was
319 not enough to expose samples from below the PAZ, as confirmed by MTLs that do not exceed the 14
320 µm. From these ages, we can only propose a minimum age for the margin erosional history that
321 should be younger than 45 Ma, i.e. the youngest AFT age accompanied by a MTL of 12.91 µm
322 (Barbarand et al., 2001). On the basis of the thermal modeling, we propose that the MTLs are more
323 sensitive to temperature and that the track length distributions may also record feeble changes in
324 cooling rate even for temperatures above the PAZ.

In order to propose a topographic evolutionary model consistent with the patterns of the thermochronological data, we tested possible thermal histories using HeFTy forward modeling (Ketcham et al., 2005). In the forward modeling approach, we tuned the T-t paths to obtain the AFT age and MTL distribution as similar as possible to the published data. The aim of this approach is to verify the hypothesis that eastern margin of the Central Massif recorded the signal of the Cenozoic uplift. Our approach of forward modeling is justified first by the absence of the single-grain AHe age and Dpar measurement from the published data, and second, because we are interested to verify if a proposed erosional history of the margin is consistent with individual sample data. In Figure 6 we show a swath profiles running perpendicular to the Cévennes (Barbarand et al., 2001) and in Figure 7 a similar profile along the NE margin (our study area) with reported the values of MTLs.

Along the Cévennes profile (Fig. 6), we choose seven samples from Barbarand et al. (2001) (n°20, 21, 22, 25, 26, 27 and 28) showing the AFT ages and track-length distributions considered as representative of the regional trend discussed in Figure 5. Thermal history of low elevation sample n°27 and n°21 (Fig. 6), showing 12.30 and 12.91 µm of MTL and AFT age of 51±2 and 45±2 Ma respectively, are consistent with a limited amount of burial during Cretaceous (up to ~96°C), a stable or slow exhumation since about 90 Ma and an increase in cooling rate starting at ~40 Ma from temperature of ~80°C. In these sample the Cretaceous phase left a weak signal because the sample was likely deep enough to not clearly record this erosion event. Sample n°22 and n°26 of Barbarand et al. (2001) are located more in the interior and should have recorded the passage of the Cenozoic erosional wave some Myr later due to the westward moving of the erosion from the base level to the margin top. Samples 22 and 21 seem very close in figure 6 because projected, and they are ~10 km far. Shorter MTLs of the sample n°22 and n°26 are consistent with this model of westward propagating erosion wave, with a longer residence in the PAZ and a younger onset of exhumation. This increase in cooling rate starts when the sample n°22 and n°21 are at ~70°C and consequently the age record a mixed age with trace of the pre-Cenozoic history. Samples n°25 and n°28 show old

cooling age, due to effect of the Cretaceous erosion event that was not enough important to bring the samples in surface, such as suggested by short MTL (very short for n°28). The last cooling is therefore induced by the Cenozoic event, concerning the cooling from ~60°C, that for this samples is younger due to progression of the erosive wave.

The uppermost sample, n°20 (Barbarand et al., 2001) shows fast cooling rate starting about 120 Ma while the pre-Cretaceous history is totally reset and not constrained (dashed lines in the modeling of n°20). Sample n°20 does not record any evidence for Cenozoic erosion because, after the Cretaceous phase, it was already near surface temperatures. Alternative thermal histories exist for each sample, but they do not explain the whole data along the profile and the relationship between MTL, elevation and age.

Now, we also verify if for the NE margin (our study area), the hypothesized Cenozoic erosion of the margin is consistent with the thermal histories of the individual samples. The NE margin, consistently with Cévennes data, shows a regular boomerang trend with long MTL on top, a decrease in the middle elevation and a slightly increase at the bottom. The trend is observable although few data are available (Fig. 5c).

Along the NE margin profile (Fig. 7), we integrated data from two published samples (n°1, n°2, Barbarand et al., 2001) with new AFT and AHe data. We followed the same approach than for the Cévennes profile, and we used forward modeling to find a T-t path as similar as possible to the obtained AFT ages and track length distribution (blue in Fig. 7). In a second step, we compare the forward modeling path with the inversion modeling obtained with QTQt software (shown in Fig. 4).

Differently from the Cévennes profile, in the NE margin the lowermost samples vo-3 and vo-21 show MTLs longer than the lowermost samples of Cévennes and Ardèche regions. The T-t path proposed for the samples vo-3 show a deeper burial (~110°C) during the Mesozoic followed by a cooling until shallow crustal level corresponding to 50° C, when they resided for ~20 Myr before being eroded since 40 to 30 Ma. Interestingly this proposed history is consistent with the inverse

thermal history proposed by QTQt software using also the AHe ages (colored paths in Fig. 7). Sample vo-4 provides shorter MTL consistent with a longer persistence at temperatures ~50° C and a younger cooling event since ~30 Ma. Although the two samples (vo-3 and vo-4) are quite close, the distance of ~5 km is considered enough to explain the difference of the MTL as being the result of the progressive propagation of the erosion wave that had reached the most internal sample some Myr later. Considering the distance of ~5 km between the two samples we can imagine that the propagation rate of the erosive wave is of the order of ~0.5 km/Myr that is consistent with escarpment retreat rate found in many continental margins (Braun, 2018).

The most internal samples (n°2 and n°1 of Barbarand et al., 2001) were not completely reset during the Cretaceous burial and preserve the heritage of the old exhumation histories. Moreover, sample n°2 being a Triassic sandstone, it further support a limited post-sedimentation erosion. In general, their short MTLs are not consistent with a Cenozoic event suggesting a regularly slow cooling. A very slight change in cooling rate at about 30 Ma can be proposed in sample n°1 only.

Another evidence supporting a Cenozoic exhumation exists such as the positive correlation of the age-elevation relationship (AER) (Fig. 3). Isotherms are influenced by topography in function of the topographic wavelength, relief amplitude and by isotherm depths (Stüwe et al., 1994; Braun, 2002; Foeken et al., 2007) so that below wide valleys (wavelengths >20-40 km) shallower isotherms tend to be parallel to the surface. A sampling profile along a valley flank of more than 10-20 km long with less than 1 km of difference in elevation, such as the case of Massif Central, is expected to yield a poor correlation between age and elevation (Braun, 2002). The observed positive correlation in the AER of the AFT and AHe data from the Massif Central suggests that relief was formed after these samples cooled below their closure temperature.

5.2 Cretaceous Pyrenean rifting

399 The Cévennes, Ardèche and NE margin (our study) areas were part of the western margin of
400 the Southeast France Basin during the Cretaceous. This sedimentary basin developed on European
401 crust since the Triassic in response to Alpine Tethys rifting. Barbarand et al. (2001) interpreted the
402 mid-Cretaceous AFT cooling ages as a general erosional event produced by an uplift commonly
403 referred to as the "Durance Uplift" event that involved the Southeast (SE) France Basin and probably
404 associated to the opening of the Gulf of Biscay. Here, we propose that mid-Cretaceous
405 thermochronological ages not only recorded the "Durance Uplift" event, but that they might reflect a
406 specific evolution of the Southeast Basin.

407 The Southeast Basin was initially NE-SW elongated in the Triassic to Middle Jurassic, being
408 parallel to the northern Tethyan paleo-margin, while since the Late Jurassic the structural trend
409 became E-W. Mid-Cretaceous corresponds to a phase of deep reorganization in the SE France basin
410 geometry, associated to a general north-south directed extensional tectonic that lead to the formation
411 of coeval "isthmus Durancien" and the formation of the two separate basins, the Vocontian basin in
412 the north and the South Provence in the south. It is possible that the erosional event, recorded in the
413 thermochronological data, was induced by the margin uplift at the transition between a subsiding and
414 extending continental domain in the east (the Vocontian Basin) and the Massif Central domain to the
415 west.

416 In the Barremian (129 to 125 Ma) the westward portion of the Vocontian trough was close to
417 the Ardèche area, while in the Albian (~110 to 100 Ma) the Vocontian trough expanded southwards,
418 toward the Cévennes, and northwards toward the NE margin (our study area) (Curnelle and Dubois,
419 1986). The younger ages found in the uppermost samples in the Cévennes and in our study area (~90
420 to 120 Ma) with respect to the older Ardèche samples (~110 to 130 Ma), might reflect the non-
421 synchronous uplift of the margin that progressively followed the basin subsidence.

422 In such a scenario, the NE-SW oriented margin of the Massif Central was oblique with respect
423 to the general N-S directed sense of extension, producing a possible transtensional tectonic regime.

The thickness of removed crust of several km, along the margin is indeed compatible with a mechanism of erosion of a transtensional uplifted rift shoulder similar to what is observed in modern continental margins. Such geodynamics context is similar to propositions for oblique continental margin, such as the Transantarctic Mountains (Wilson 1995).

The importance of the mid-Cretaceous extensional phase, associated to the Bay of Biscay - Pyrenean rift, is highlighted by large geological evidence in the SE basin and recently found also in the Western Alps (Tavani et al., 2018 and references therein).

5.3 Cenozoic uplift

The hypothesis of a Cenozoic age for the eastern Massif Central topography is supported by thermal and topographic evolution derived from our and published data. The "boomerang" trend of the MTL-age and MTL-elevation relationships (Fig. 5) are the most convincing evidence for a Cenozoic uplift-induced erosion of the margin, that is supported by the thermal inverse and forward modeling.

The massif margin may be considered as a smaller scale analogue to an elevated continental passive margin, with comparable erosional pattern due to a regressive erosion wave moving from the bottom to the top following a Cenozoic uplift phase. The base level is represented by the Rhône river that contributed to maintain the main valley floor at the same elevation during the Cenozoic. The limited amount of erosion coupled with the general eastward tilting of the Cretaceous formations and no evidence for faulting suggest a topographic evolution similar to a downwarp model of a continental shoulder evolution (Ollier and Pain, 1997). This model implies a long wavelength flexure of the lithosphere, which produces a margin topography characterized by a broad monocline with a very low gradient (see Gallagher and Brown 1998; Wildman et al., 2018). In the case of the Massif Central, no Cenozoic extensional rifting domain is invoked to produce the uplift, but such an erosional model is consistent with a long wavelength topographic growth induced by mantle

449 upwelling, providing a remarkable consistency with the deep and localized present-day high
450 temperature anomaly imaged by seismic tomography (Granet et al., 1995; Faccenna et al., 2014) and
451 the long-term surface evolution. Volcanism is another evidence for mantle involvement during
452 topographic growth, with the first activity attested about 30 Ma and an effusive acme since 15 Ma
453 (Michon and Merle, 2001).

454 The age onset for the uplift is not well constrained by our thermochronology data. The
455 Cenozoic event recognized in the MTL regional distribution and supported by forward modeling
456 should have occurred after ca. 45 Ma (AFT age of the youngest sample in the Cévennes area,
457 Barbarand et al., 2001) although it remains difficult to precisely constrain because of limited erosion
458 and dispersed AHe ages. Lutetian (48 to 40 Ma) marine deposits have been described in several
459 basins located in the middle of the massif, such as the Puy Basin (Seranne et al., 2001; Michon, 2000
460 and references therein) testifying that margin uplift occurred not before ~40 Ma (Fig. 8a).

461 Between late Eocene and Oligocene, some portions of the Massif Central have been involved in
462 two regional extensional events: the European rifting and the opening of the Gulf of Lion. The
463 European rifting is associated to localized crustal extension within individual basins, such as Bresse
464 basin, while a coeval uplift and erosional event at regional scale has been never described. The
465 amount of uplift and volcanic activity in Massif Central are much higher than in other analogue
466 massifs (e.g. Vogelsberg mountains, Rhine and Bohemian massifs), suggesting the contribution of
467 other processes. The opening of Gulf of Lion (30 to 16 Ma) (Fig. 8c) corresponds to an important
468 tectonic phase that reactivated Paleozoic structures such as the Nimes fault and in general deeply
469 reshaped the western Mediterranean plate organization (Séranne et al., 1995). The onset of the
470 margin uplift could have been started at the beginning of this re-organization event.

471 The Massif Central plume in the early Miocene probably interacted with the Ionian subduction
472 system that contributed to continuously nourishing the mantle upwelling and flow. The contribution
473 of the Ionian subduction in the Massif Central volcanism has been already proposed (Barruol and

Granet 2002; Faccenna et al., 2010) and also supported by seismic anisotropy (Faccenna et al., 2014; Salimbeni et al., 2018) that imaged well the northwest-southeast directed mantle counter-flow induced by Ionian slab retreat during the opening of Gulf of Lion (Fig. 8c). The interaction of the Massif Central mantle plume with the slab retreat induced counter-flow could have caused the greater volcanism, the higher total elevation and the long-term slow surface uplift evolution of the Massif Central.

The amount of exhumation and of margin uplift is also uncertain; if we consider the thermal modeling consistent with a progressive westward erosion of the margin (Figs. 6-7) we can observe that samples cooled by ~40° C during the last 30-40 Ma, corresponding to a removal of about 1 km of crustal thickness (assuming a geothermal gradient of 30°/km). These numbers allow to propose exhumation (and uplift) rate ranging from 0.025 to 0.033 mm/yr (Fig. 8c) which is comparable with modern basin-averaged cosmogenic denudation rates reported in the area (about 0.04 mm/yr, Olivetti et al., 2016), suggesting that a large portion of the slowly-eroding landscape underwent a constant process of erosion during the last 40 Myr. Other portions of the landscape are eroding slightly faster (cosmogenic denudation rate of 0.07 mm/yr), suggesting that uplift might have further increased and it is probably still active today. The more recent higher denudation rates are consistent with the inferred uplift rate from the elevation of a Pliocene marine-continental transition deposits found along the Rhône valley, at 200 m asl (Peage de Roussillon village, Fig. 3)(Aguilar et 1989).

6. Conclusions

Our new thermochronological study from the eastern margin of the French Massif Central, along with literature data, permits to reconstruct the long-term evolution of long-wavelength topography. A two-step history has been recorded in the regional data trends: i) a first mid-Cretaceous exhumation phase ii) a second, newly-recognized, Cenozoic erosional phase affecting the newly-formed margin with onset time likely after the Eocene. For this Cenozoic phase, we envisage a

499 domal uplift of the area at least partly due to mantle upwelling with the formation of a long
500 wavelength flexure at the margin and subsequent erosion of the scarp. The total amount of erosion is
501 limited, such that AHe and AFT ages exposed by the erosional wave, do not record the onset of the
502 phase but released mixed ages. On the contrary, AFT, track-length data and thermal modeling permit
503 to record the signal of a post-50 Ma event of erosion induced by a progressive westward regressive
504 erosion starting at the eastern margin of the massif.
505
506 Acknowledgements
507 Research and post-doctoral allocation of V.O. were funded by EDF (Electricité De France)
508 through the SIGMA research program (SeIsmic Ground Motion As-sessment). This work is also a
509 contribution of the ECCOREV research federation and Labex OT-Med (ANR-11-LABX-0061)
510 funded by the French Government "Investissements d'Avenir" program of the French National
511 Research Agency (ANR) through the A*MIDEX project (ANR-11-IDEX-0001-02). P.G.V.
512 acknowledges support from Swiss National Science Foundation (SNSF) grant PP00P2_170559.
513
514 Appendix
515 A1. Apatite Thermochronology
516 The apatite grains were recovered from the collected samples following standard crushing,
517 sieving, washing, magnetic, and heavy liquid separation.
518 A1.1. Apatite Uranium-Thorium/Helium Thermochronology
519 The AHe analyses were carried out at the Paris-Sud University. Euhedral apatites were picked
520 using a cross polarized binocular microscope. Most grains had a minimum diameter of 90 μm and
521 were inclusion free to avoid effects of He-implanting from inclusions or excess loss of He during
522 decay due to a large surface/volume ratio (Farley, 2000). The grain dimensions were measured for
523 calculation of the alpha-ejection (Ft) correction factor after Farley et al. (1996), and single grains

were packed in Nb-tubes for U-Th/He measurement. For each sample up to five aliquots were prepared for analysis in order to ensure sample age reproducibility. The concentration of ^{4}He was determined by the ^{3}He isotope dilution and measurement of the $^{4}He/^{3}He$ ratio through a quadrupole mass spectrometer. Apatite samples were heated for 5 min at 11 Amps with a 960 nm diode laser for degassing. Each sample was reheated and measured to ensure that all gas was extracted in the first run. U, Th concentrations were obtained by isotope dilution using an inductively coupled plasma mass spectrometer.

A1.2. Apatite Fission Track thermochronology (AFT)

Apatite grains were mounted in epoxy resin, ground, and polished to expose internal mineral surfaces. Etching with 5 N HNO_3 at room temperature for 20 s revealed spontaneous fission tracks intersecting the apatite surface. Samples were covered with a uranium free muscovite external detector and irradiated with thermal neutrons at the LENA (Laboratorio Energia Nucleare Applicata) Triga Mark II reactor of the Pavia University, Italy. Induced fission tracks in the external detector were revealed by etching the mounts in 40% HF at room temperature for 40 min. The fission tracks were counted by the first author under a nominal magnification of 1250X on a Zeiss Axioskop equipped with a Kinetek automatic stage at the CNR-IGG Fission-Track laboratory. The Trackkey 4.2 Program was used for all AFT age calculations procedures (Dunkl, 2002). A chi-square ($\chi 2$) test is carried out on the AFT single-grain age in order to test the homogeneity of data (Galbraith, 1981). The probability of ($\chi 2$) is calculated for each sample; if $P(\chi 2) > 5\%$ then the sample is assumed to be homogenous (Galbraith and Laslett, 1993).

References

Aguilar, J.P., Clauzon, G. and Michaux, J., 1989, La limite Mio-Pliocène dans le Sud de la France d'après les faunes de rongeurs; état de la question et remarques sur les datations à l'aide des rongeurs: Bollettino della Società Paleontologica Italiana, v. 28(2/3), p.137-145.

549 Alabouvette, B., and Cavelier, C., 1984, Languedoc oriental, in Chapitre Paléogène. in: S. Debrandpassard and S.
550 Courbouleix, eds., Synthèse géologique du Sud-Est de la France – Stratigraphie et paléogéographie: BRGM,
551 Orléans, France, Mém. n°125, 434-438.
552 Ambert P., 1994, L'évolution géomorphologique du Languedoc central depuis le Néogène (Grands Causses méridionaux
553 – piémont languedocien. *Doc.* BRGM, 231, 210.
554 Balestrieri, M.L., Pandeli, E., Bigazzi, G., Carosi, R., and Montomoli, C., 2011, Age and temperature constraints on
555 metamorphism and exhumation of the syn-orogenic metamorphic complexes of Northern Apennines, Italy:
556 Tectonophysics, v. 509(3-4), p. 254-271.
557 Barbarand, J., Lucazeau, F., Pagel, M., and Séranne, M., 2001, Burial exhumation history of the southern–eastern Massif
558 Central (France) constrained by apatite fission-track thermochronology: Tectonophysics, v. 335, p. 275–290.
559 Blés, J.L., Bonijoly, D., Castamg, C., Gras, Y., 1989. Successive post-Variscan stress fields in the French Massif Central
560 and its borders (Western European plate): comparison with geodynamic data. Tectonophysics169, 79–111.
561 Braun, J., 2002. Quantifying the effect of recent relief changes on age–elevation relationships: Earth and Planetary
562 Science Letters, v. 200, p. 331-343.
563 Braun, J., 2018, A review of numerical modeling studies of passive margin escarpments leading to a new analytical
564 expression for the rate of escarpment migration velocity: Gondwana Research, v. 53, p. 209-224.
565 Chantraine, J., Autran, A. and Cavelier, C., 2003, Carte géologique de la France à 1/1 000 000 6ème édition révisée.
566 BRGM, Orléans.
567 Clauzon, G., 1982, The Messinian Rhone canyon as a definite proof of the desiccated deep-basin model: Bulletin de la
568 Société Géologique de France, v. 24(3), p.597-610.
569 Curnelle, R., and Dubois, P., 1986, Évolution mésozoique des grands bassins sédimentaires Français; bassins de Paris,
570 d'Aquitaine et du Sud-Est: Bulletin de la Société Géologique de France, v. 2, p. 529–546.
571 Define, E., and Cantagrel, J.M., 1998, Chronologie de l'encaissement du réseau hydrographique en domaine volcanisé:
572 l'exemple de la haute vallée de la Loire. INQUA COT/UISPP 31 Inter-congress Symposium, Brives-Charensac,
573 12-17.
574 Djimbi, D.M., Gautheron, C., Roques, J., Tassan-Got, L., Gerin, C. and Simoni, E., 2015, Impact of apatite chemical
575 composition on (U-Th)/He thermochronometry: an atomistic point of view: Geochimica et Cosmochimica Acta, v.
576 167, p. 162-176.
577 Dunkl, I., 2002, Trackkey: a Windows program for calculation and graphical presentation of fission track data: Computer
578 Geoscience, v. 28 (1), p. 3–12.

579 Etienne, R., 1970, Les Monts du Forez. Le rôle de l'érosion différentielle et de la tectonique dans l'édification du relief :
580 Thèse 3ème cycle, Univ. Clermont Ferrand, 183.
581 Faccenna, C., Becker, T., Lallemand, S., Lagabrielle, Y., Funiciello, F., and Piromallo, C., 2010, Subduction-triggered
582 magmatic pulses: a new class of plumes?: Earth and Planetary Science Letters, v. 299(1), p. 54–68.
583 http://dx.doi.org/10.1016/j.epsl.2010.08.012.
584 Faccenna, C., Becker, T.W., Auer, L., Billi, A., Boschi, L., Brun, J.P., Capitanio, F.A., Funiciello, F., Horvath, F., Jolivet,
585 L., Piromallo, C., Royden, L.H., Rossetti, F., and Serpelloni, E., 2014, Mantle dynamics in the Mediterranean.
586 Review of Geophysics, v. 52, p. 283–332
587 Foeken, J.P.T., Persano C., Stuart F.M., and ter Voorde, M., 2007, Role of topography in isotherm perturbation: Apatite
588 (U-Th)/He and fission track results from the Malta tunnel, Tauern Window, Austria: Tectonics, v. 26. doi: 10
589 .1029 /2006TC002049
590 Gallagher, K. and Brown, R., 1999, Denudation and uplift at passive margins: the record on the Atlantic Margin of
591 southern Africa. Philosophical Transactions of the Royal Society of London. Series A: Mathematical, Physical and
592 Engineering Sciences, v. 357(1753), p. 835-859.
593 Gallagher, K., 2012, Transdimensional inverse thermal history modeling for quantitative thermochronology: Journal of
594 Geophysical Research, v. 117. https://doi.org/10.1029/2011JB008825
595 Gautheron, C., Tassan-Got, L., Barbarand, J., and Pagel, M., 2009, Effect of alpha-damage annealing on apatite (U–
596 Th)/He thermochronology: Chemical Geology, v. 266, p. 157-170.
597 Girod M., Bouiller R., Roche A., Weber F., Larque P. Giot D., Guerin C., Bladier Y., Laurent Ph., and Bambier A., 1979,
598 Carte géologique de la France au 1/50000: notice du Puy en Velay. *Ed B.R.G.M*., 31.
599 Green, P.F., 1986, On the thermo-tectonic evolution of northern England: evidence from fission track analysis.
600 Geological Magazine, v. 153, p. 493–506.
601 Ketcham, R.A., 2005, Forward and inverse modeling of low-temperature thermochronometry data, Reviews in
602 mineralogy and geochemistry, v. 58 (1), p. 275–314.
603 Ketcham, R.A., Carter, A., Donelick, R.A., Barbarand, J. and Hurford, A.J., 2007, Improved modeling of fission-track
604 annealing in apatite: American Mineralogist, v. 92(5-6), p. 799-810.
605 Le Griel, A., 1988, L'évolution géomorphologique du massif central français. Essai sur la genèse d'un relief. Thèse d'état,
606 Univ. Lyon II, 2 vol., 569.
607 Lucazeau, F., Vasseur, G., and Bayer, R., 1984, Interpretation of heat flow data in the French Massif
608 Central: Tectonophysics, v. 103, p. 99-119.

Mahéo, G., Gautheron, C., Leloup, P.H., Fox, M., Tassan-got, L. and Douville, E. 2013. Neogene exhumation history of the Bergell massif (southeast Central Alps): Terra Nova, v. 25, p. 110-118.

Michon L., 2000. Dynamique de l'extension continentale-Application au Rift Ouest-Européen par l'étude de la province du Massif Central, Ph.D. Thesis, Université Blaise Pascal, Clermont-Ferrand.

Michon, L., and Merle, O. 2001, The evolution of the Massif Central Rift; spatio-temporal distribution of the volcanism: Bullettin de la Societé Géologique de France, v. 172(2), p. 201-211.

Olivetti, V., Godard, V., Bellier, O., and ASTER Team, 2016, Cenozoic rejuvenation events of Massif Central topography (France): Insights from cosmogenic denudation rates and river profiles: Earth Planetary Science Letters, v. 444, p. 79-191.

Ollier, C.D., and Pain, C.F., 1997, Equating the basal unconformity with the palaeoplain: a model for passive margins: Geomorphology, v. 19 (1–2), p. 1–15.

Peyaud, J.B., Barbarand, J., Carter, A., and Pagel, M., 2005, Mid-Cretaceous uplift and erosion on the northern margin of the Ligurian Tethys deduced from thermal history reconstruction: Internation Journal of Earth Science, v. 94 (3), p. 462–474.

Recanati, A., Gautheron, C., Barbarand, J., Missenard, Y., Pinna-Jamme, R., Tassan-Got, L., Carter, A., Douville, E., Bordier, L., Pagel, M. and Gallagher, K., 2017, Helium trapping in apatite damage: Insights from (U-Th-Sm)/He dating of different granitoid lithologies, Chemical Geology, v. 470, p. 116-131.

Rey R., 1971, Biostratigraphie des bassins tertiaires du Massif Central. In: Géologie, Géomorphologie et Structure Profonde du Massif Central français. Symposium J. Jung. Plein Air Service , Clermont Ferrand, 309-330.

Salimbeni S., Malusà, M.G., Zhao L., Guillot S., Pondrelli S., Margheriti L., Paul A., Solarino S., Aubert C., Dumont T., Schwartz S., Wang Q., Xu X., Zheng T., and Zhu R., 2018, Active and fossil mantle flows in the western Alpine region unravelled by seismic anisotropy analysis and high-resolution P wave tomography : Tectonophysics, v. 35, p. 731–732.

Scotti, V.N., Molin, P., Faccenna, C., Soligo, M. and Casas-Sainz, A., 2014, The influence of surface and tectonic processes on landscape evolution of the Iberian Chain (Spain): Quantitative geomorphological analysis and geochronology: Geomorphology, v. 206, p.37-57.

Séranne, M., Benedicto. A., Labaum, P., Truffertt, C., and Pascal, G., 1995, Structural style and evolution of the Gulf of Lion Oligo-Miocene rifting: role of the Pyrenean Orogeny: Marine Petroleum Geology, v. 12, p. 809-820,

637 Séranne, M., Camus, H., Lucazeau, F., Barbarand, J., and Quinif, Y., 2002, Surrection et érosion polyphasées de la
638 bordure cévenole : Un exemple de morphogenèse lente. Bullettin de la Societé Geologique de France, v. 173 (2),
639 p. 97–112.
640 Shuster, D.L., Flowers, R.M. and Farley, K.A., 2006, The influence of natural radiation damage on helium diffusion
641 kinetics in apatite: Earth and Planetary Science Letters, v. 249(3-4), p. 148-161.
642 Sissingh, W. 1998, Comparative Tertiary stratigraphy of the Rhine Graben, Bresse Graben and Molasse Basin:
643 correlation of Alpine foreland events: Tectonophysics, v. 300, p. 249-284.
644 Stanley, J.R., Flowers, R.M. and Bell, D.R., 2013, Kimberlite (U-Th)/He dating links surface erosion with lithospheric
645 heating, thinning, and metasomatism in the southern African Plateau: Geology, v. 41(12), p. 1243-1246.
646 Stuwe, K., White, L., and Brown R.W., 1994, The influence of eroding topography on steady state isotherms. Application
647 to fission track analysis: Earth and Planetary Science Letters, v. 124, p. 63-74.
648 Tesauro, M., Kaban, M.K., and Cloetingh, S.A., 2008, EuCRUST-07: A new reference model for the European
649 crust: Geophysical Research Letters, v. 35(5).
650 Turland, M., Marteau, P., Jouval, J., and Monciardini, C., 1994, Découverte d'un épisode marin oligocène inférieur dans
651 la série paléogène lacustre à fluviatile du bassin du Puy-en-Velay (Haute-Loire), Géologie de France, v. 4, p. 63-
652 66.
653 Vernon, A.J., Van Der Beek, P.A., Sinclair, H.D., Persano, C., Foeken, J., and Stuart, F.M., 2009, Variable late Neogene
654 exhumation of the central European Alps: Low-temperature thermochronology from the Aar Massif, Switzerland,
655 and the Lepontine Dome, Italy: Tectonics, v. 28(5).
656 Wildman, M., Cogné, N., Beucher, R., 2018. Fission-Track thermochronology applied to the evolution of passive
657 continental margins. In M. G. Malusà & P. G. Fitzgerald (Eds.), Fission-Track thermochronology and its
658 application to geology (351– 371). Cham: Springer.
659 Wilson, T.J., 1995, Cenozoic transtension along the Transantarctic Mountains-West Antarctic rift boundary, southern
660 Victoria Land, Antarctica: Tectonics, v.14(2), p.531-545.
661 Wyns, R., and Guillocheau, F., 1999, Géomorphologie grande longueur d'onde, altération, érosion et bassins
662 épicontinentaux. in: P. LEDRU, eds. Colloque GéoFrance 3D - résultats et perspectives. - BRGM, 293, 103-108.
663 Wyns, R., Quesnel, F., Simon-Coinçon, R., Guillocheau, F., and Lacquement, F., 2003, Major weathering in France
664 related to lithospheric deformation: Géologie de France, 1(7).
665
666

667 **Figure captions**

668 Figure 1. (a) Topographic setting and main tectonic features of the West Mediterranean sea. (b)
669 Topography of the French Massif Central, and (c) filtered topography at 50 km wavelength. The
670 locations of two swath profiles are shown. (d) Maximum, minimum and mean topography along the
671 two profiles, the yellow lines correspond to the 50km filtered topography.

672

673 Figure 2. (a) Geological map of the French Massif Central. (b) Main tectonic events and
674 corresponding vertical crustal movements. (c) Age-elevation relationships from literature data and
675 apparent exhumation rate from linear regression. Locations are shown on the map.

676

677 Figure 3. (a) Topographic map showing the sampling location and thermochronological ages.
678 (b) Age-elevation relationship of the AFT and single grain AHe ages from this study and from
679 Barbarand et al., 2001 (two samples) .

680

681 Figure 4. Time-temperature history paths obtained from QTQt inverse thermal modeling of the
682 AFT and AHe data. For each model, the comparison of the modeled vs obtained data are shown (note
683 the onset in elevation between AHe replicates is only for visual clarity). For details of the different
684 statistical models, see Gallagher (2012).

685

686 Figure 5. Mean track length (MTL) against elevation for the (a) Cévennes and (b) Ardèche
687 literature data and for the (c) new data. The blue zones represent samples which recorded the old and
688 fast erosional history only (mid Cretaceous phase), the white zones represents samples which
689 recorded a slow erosion since the Cretaceous, and the green zones represent samples that could have
690 recorded a slightly faster Cenozoic erosion. (d) AFT and MTL relationships for the new (pink) and

691 literature data showing a possible boomerang trend given by the slight increasing MTLs in the
692 younger samples.
693
694 Figure 6. Mean track length regional distribution along the EW swath profiles of the Cévennes.
695 In the inserted boxes: the grey lines show the modelled time-temperature histories compatible with
696 the published data of MTL and AFT ages, whose values are reported in black; histogram shows the
697 distribution of the measured track length from published data (Barbarand et al., 2001); red curve
698 represents the track length probability distribution from forward modeling; in red the modelled MTL
699 and AFT age are reported.
700
701 Figure 7. Mean track length regional distribution along the EW swath profiles of the NE margin
702 (our study area). In the inserted boxes: the grey lines show the modelled time-temperature histories
703 compatible with the published data of MTL and AFT ages, whose values are reported in black;
704 histogram shows the distribution of the measured track length from published data (Barbarand et al.,
705 2001); red curve represents the track length probability distribution from forward modeling; in red
706 the modelled MTL and AFT age are reported. For the new data, the inverse modeling is shown (given
707 in Figure 4).
708
709 Figure 8. Summary of the Cenozoic vertical movement history deduced by
710 thermochronological data and geological constraints. (a) A possible landscape after the Cretaceous
711 uplift and before the Cenozoic rejuvenation. (b) A first event of Cenozoic regional uplift inducing a
712 lithospheric flexures and a downwarped margin. (c) A second event of uplift, maybe slightly faster,
713 and recorded in the increased denudation rates and river incision. (d) Comparison of the long-term
714 erosion rate from thermal modeling of the thermochronological data with the short-term denudation

715 rate from cosmogenic nuclides and with the uplift rate from marine deposits (Olivetti et al., 2016).
716 The main geological events are shown.
717
718 Table 1 Apatite (U-Th-Sm)/He data
719 Notes: crystal weight has been determined using the Ca content. eU: effective uranium, Rs:
720 equivalent spherical radius: FT is the α-ejection correction after Ketcham et al., (2011).
721
722 Table 2 Apatite fission-track data
723 Notes - Ages determined by external detector method using a zeta value for dosimeter CN5 $\zeta = 360 \pm$
724 11 (referred to Fish Canyon Tuff and Durango apatite standards, Hurford, 1990). El (m): sample
725 elevations in metres; ρd, ρi: standard and induced track densities measured on mica external
726 detectors; ρs: spontaneous track densities on internal mineral surfaces, track densities are given in
727 105 tracks cm-2; nd, ni and ns: number of tracks on external detectors and on mineral surfaces; ng:
728 number of counted mineral grains; P(χ2): (χ2) probability (Galbraith, 1981); Central age calculated
729 using TRACKKEY program (Dunkl, 2002); Lm: mean length of confined tracks length distribution ±
730 standard error, s.d.: standard deviation, nTINTs: number of measured lengths; only TINTs (tracks
731 reached by the etching because they intercept a surface track, Bhandari et al., 1971) were measured,
732 as recommended by Ketcham (2005). Dpar: mean etch pit diameter parallel to the c-axis and number
733 of total measured Dpar for sample; Samples were irradiated in the Lazy Susan facility of the Triga
734 Mark II reactor of the LENA, University of Pavia (Italy).

Figure 1

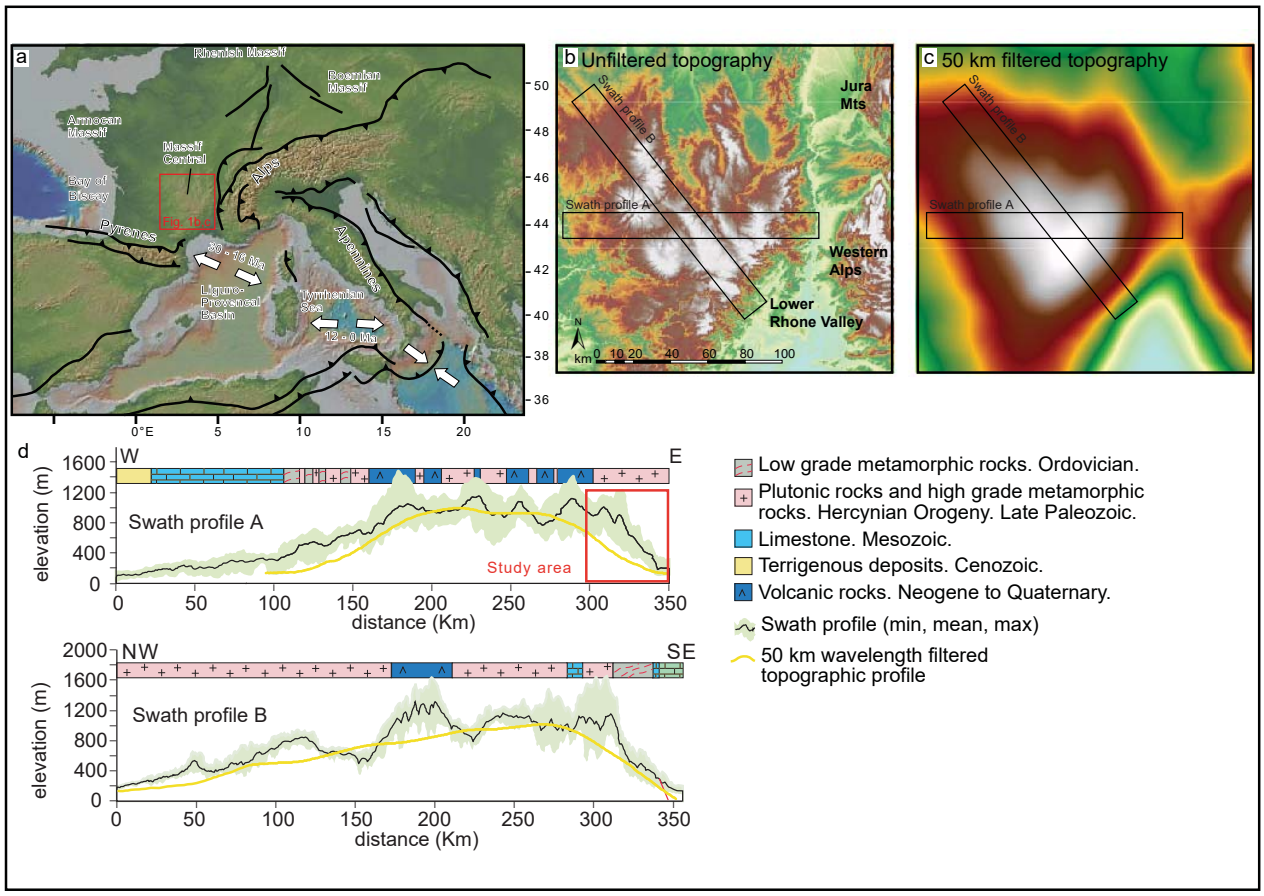


Figure 1

Figure 2

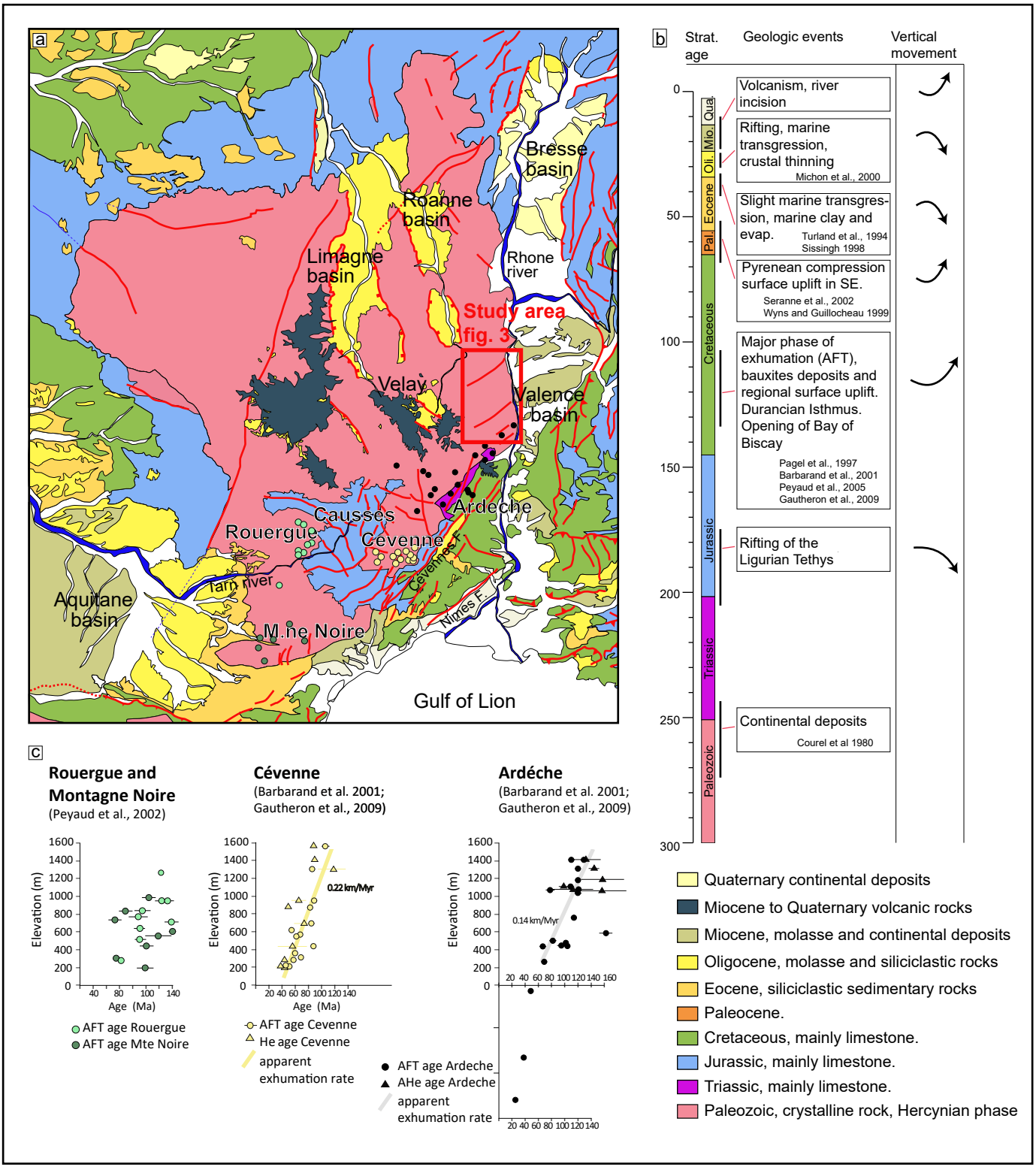


Figure 2

Figure 3

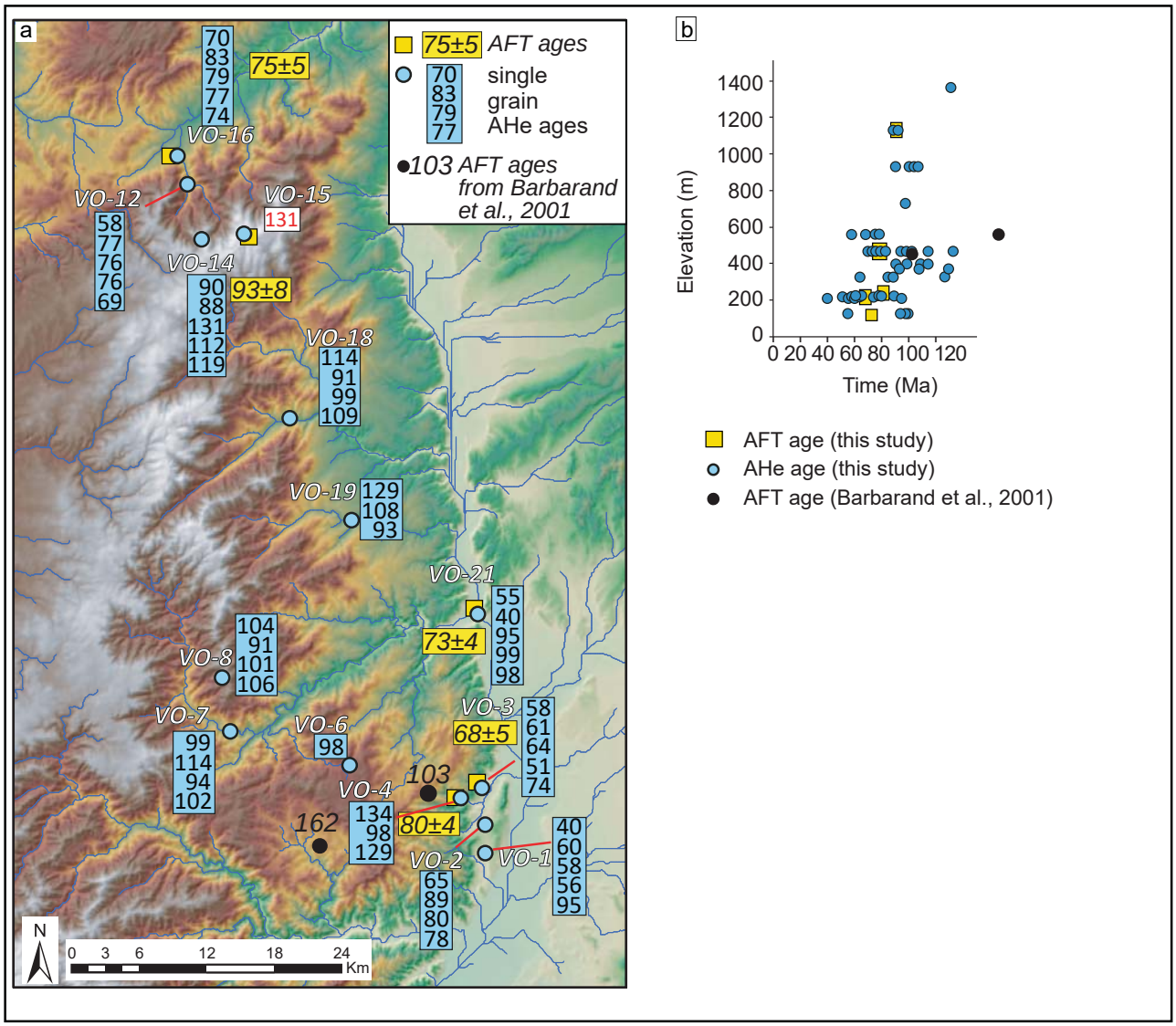


Figure 3

Figure 4

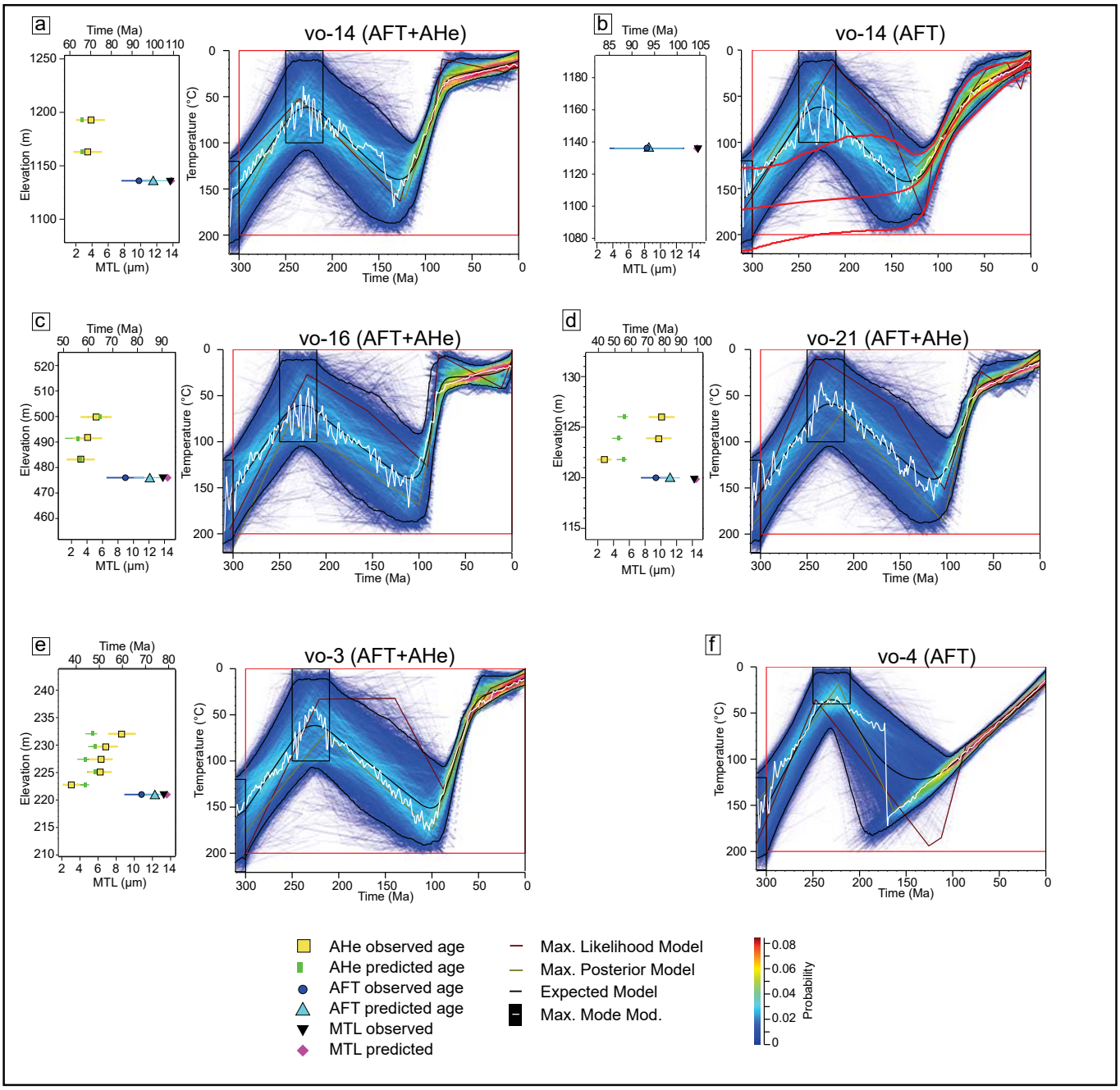


FIGURE 4

Figure 5

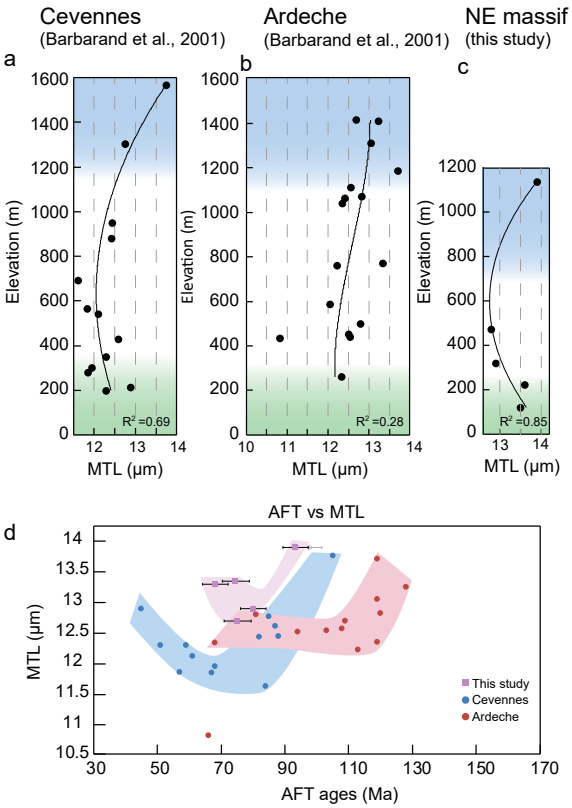


Figure 5

Figure 6

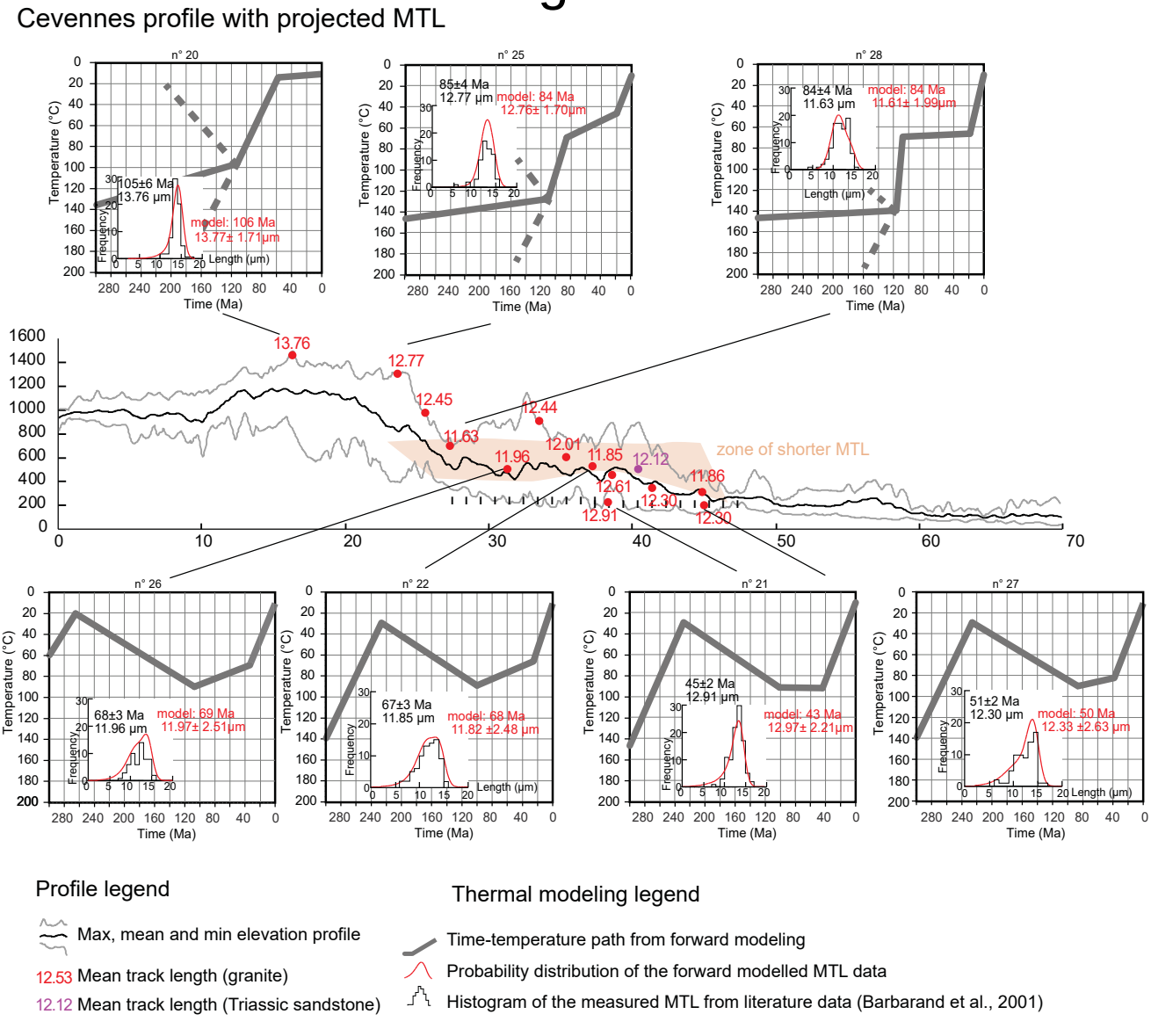


figure 6

Figure 7

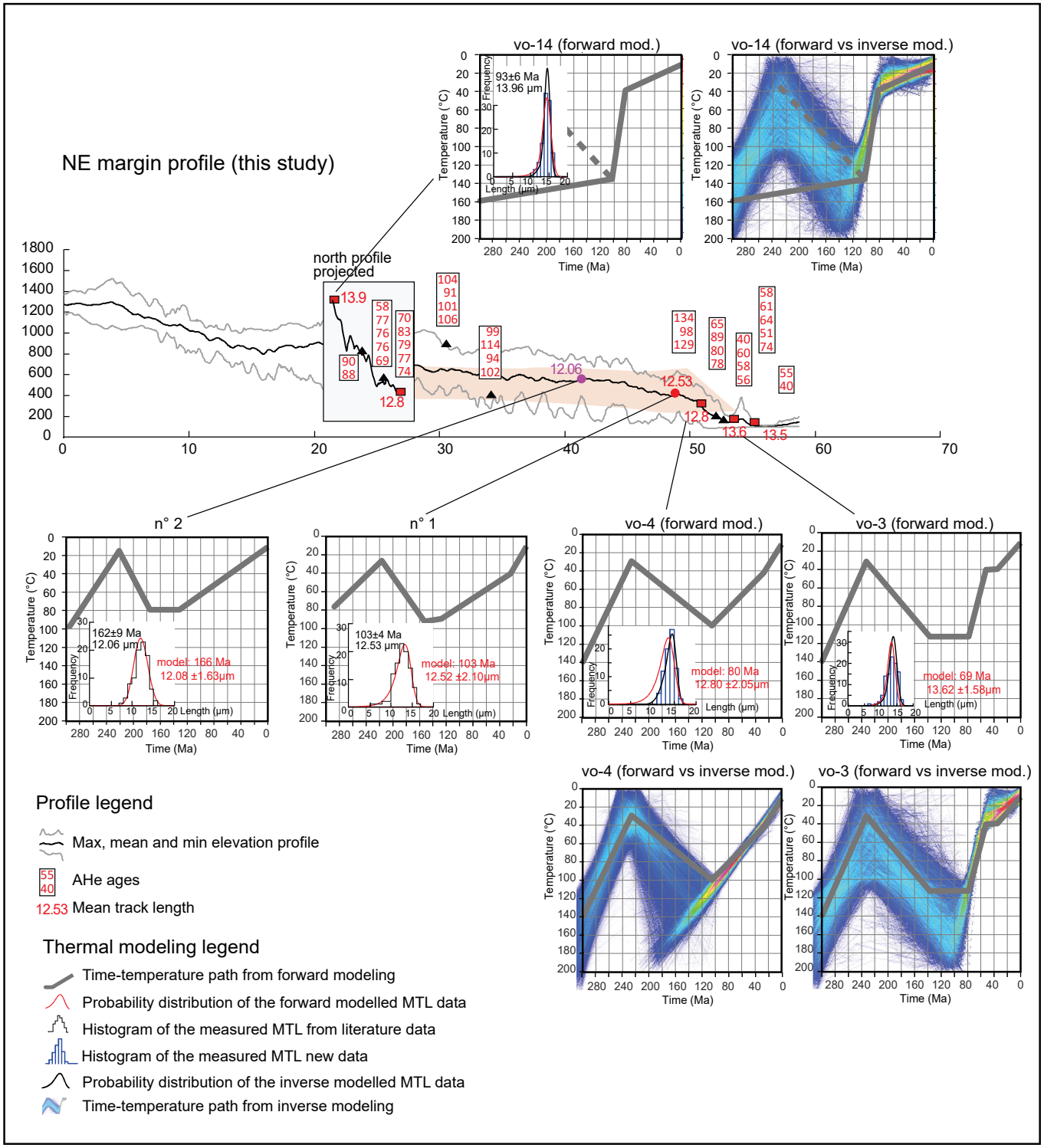


figure 7

Figure 8

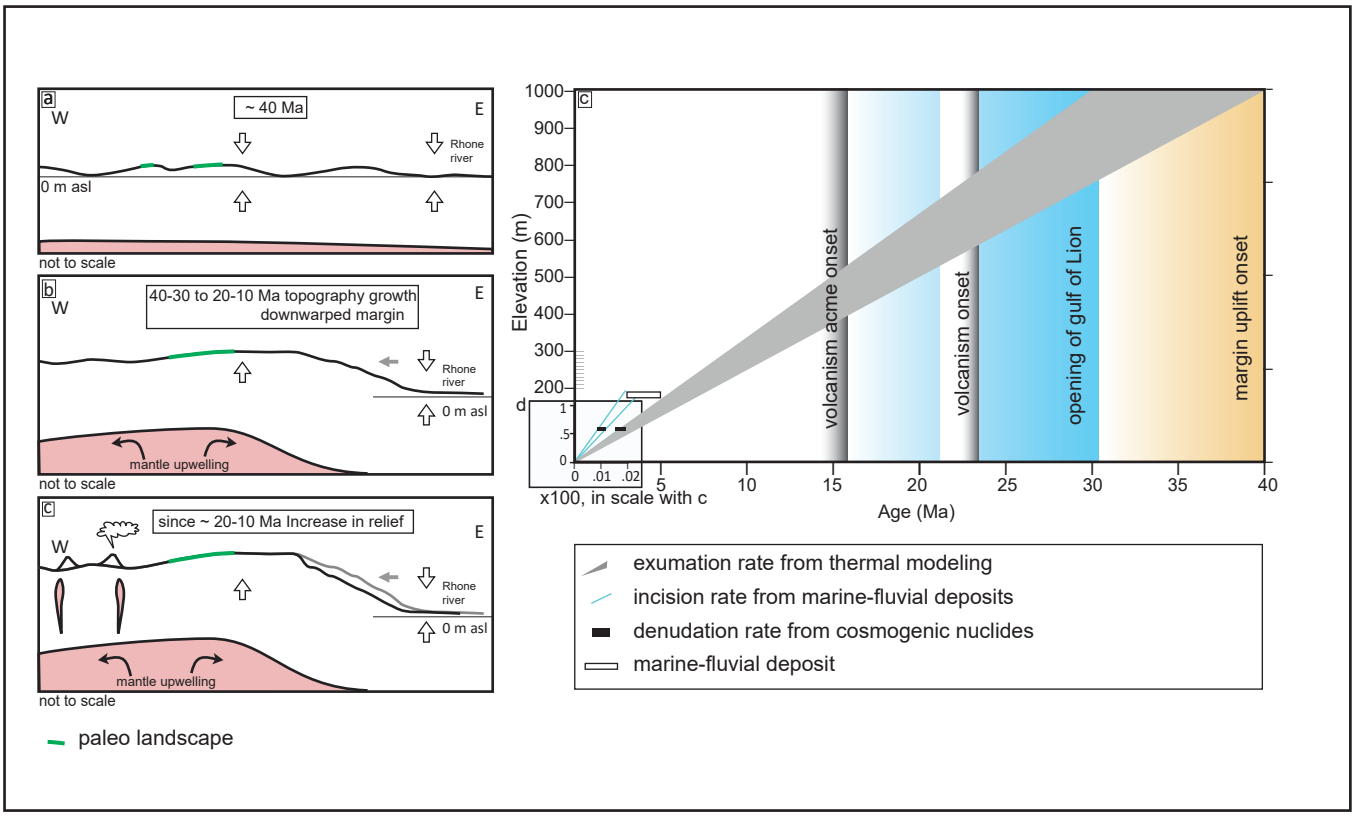


Figure 8

Sample	Elevation	Length	Width	Tickness	Weight	Rs	FT	^{4}He	U	Th
	m asl	µm	µm	µm	mg	µg		ncc/g	ng	ng
VO-1A	203	158	111	88	3.0	52.8	0.76	1.90E+05	0.1449	0.0184
VO-1B	203	164	115	109	3.8	57.0	0.78	6.11E+05	0.3896	0.0608
VO-1C	203	184	105	80	3.3	52.2	0.73	3.64E+05	0.2197	0.0448
VO-1D	203	283	175	135	11.2	76.5	0.81	2.75E+05	0.5424	0.0592
VO-1E	203	287	164	138	13.1	84.0	0.83	6.01E+05	0.7814	0.1644
VO-2A	217	193	119	89	4.2	57.7	0.75	5.02E+05	0.3290	0.1131
VO-2B	217	199	124	112	5.3	63.2	0.77	1.10E+06	0.6824	0.0524
VO-2D	217	195	101	98.7	3.8	54.7	0.77	1.02E+06	0.5078	0.0380
VO-2E	217	187	102	95.1	3.6	54.1	0.76	1.04E+06	0.4932	0.1161
VO-3A	213	156	137	117	6.0	64.2	0.81	1.40E+05	0.1280	0.0451
VO-3B	213	103	131	99	3.3	53.0	0.78	1.45E+05	0.0675	0.0466
VO-3C	213	161	125	123	5.7	62.4	0.80	2.07E+05	0.1704	0.0514
VO-3D	213	156	95	88	3.1	49.6	0.74	1.87E+05	0.0936	0.1205
VO-3E	213	162	121	108	5.0	59.7	0.79	2.90E+05	0.1791	0.0820
VO-4A	323	147	84	71	2.1	43.5	0.71	6.76E+05	0.0578	0.0165
VO-4B	323	122	75	70	1.5	39.2	0.68	7.13E+05	0.0552	0.0363
VO-4C	323	185	91	89	2.9	49.9	0.72	5.45E+05	0.1194	0.0408
VO-4D	323	99	78	68	1.3	37.8	0.80	4.85E+05	0.0544	0.0389
VO-4E	323	133	76	67	1.6	39.8	0.68	1.66E+06	0.0868	0.0458
VO-4F	323	117	103	66	1.6	42.5	0.72	5.68E+05	0.0737	0.0120
VO-6D	725	299	112	104	8.2	63.8	0.79	1.04E+04	0.0061	0.0126
VO-7A	463	188	115	99	4.2	58.2	0.76	7.43E+05	0.3318	0.0293
VO-7B	463	146	125	103	3.5	56.2	0.75	7.60E+05	0.2379	0.0580
VO-7C	463	229.5	156	153	10.0	78.7	0.82	1.05E+06	0.7732	0.0548
VO-7D	463	170	113	105	3.8	56.8	0.75	7.13E+05	0.3033	0.0324
VO-7E	463	225	132	117	8.3	68.8	0.81	6.93E+05	0.5608	0.0299
VO-8A	928	178.5	99	87	3.7	52.0	0.73	1.37E+06	0.5384	0.0331
VO-8B	928	129.5	97	78	2.4	46.6	0.70	9.63E+05	0.2490	0.2053
VO-8C	928	90.5	105	97	2.2	46.0	0.75	1.43E+06	0.2961	0.7912
V0-8D	928	131	110	78	2.2	47.8	0.71	1.83E+06	0.4559	0.0263
VO-8E	928	168.5	119	81	3.4	53.9	0.74	1.07E+06	0.3492	0.1198
VO-12A	556	137	134	117	5.1	61.3	0.80	1.76E+04	0.0118	0.0152
VO-12B	556	139.5	112	99	3.7	54.2	0.77	2.16E+05	0.0951	0.0501
VO-12C	556	198	92	75	3.3	48.9	0.71	3.24E+05	0.1327	0.1178
VO-12D	556	221.5	105	97	5.3	57.5	0.77	2.25E+05	0.1307	0.1351
VO-12E	556	296.5	220	202	24.2	106.5	0.88	3.74E+04	0.1174	0.0123
VO-14A	1123	164.5	114	100	3.6	55.9	0.75	4.64E+05	0.1645	0.1425
VO-14B	1123	138	119	114	4.3	57.5	0.76	229389.5	0.105	0.052
VO-14C	1123	151	117	75	3.5	51.7	0.73	4.94E+05	0.1387	0.0234
VO-14D	1123	132	126	89	3.8	54.6	0.74	3.24E+05	0.1101	0.0325
VO-14E	1123	137	108	76	2.9	49.1	0.75	4.93E+05	0.1227	0.0216
VO-15D	1358	102	77	62	0.9	36.0	0.62	4.19E+05	0.0300	0.0263
VO-16A	461	129.5	111	103	3.5	53.4	0.74	1.97E+05	0.0955	0.0415
VO-16B	461	215.5	154	108	9.2	71.6	0.80	2.09E+05	0.2279	0.0222
VO-16C	461	132	116	82	3.2	51.5	0.73	2.13E+05	0.0872	0.0273
VO-16D	461	339	145	110	13.5	76.2	0.82	2.71E+05	0.4718	0.0087
VO-16E	461	131.5	106	98	3.2	51.8	0.73	1.75E+05	0.0780	0.0164
VO-18A	392	114.5	106	94	2.7	49.4	0.72	7.93E+05	0.2031	0.0331
VO-18C	392	191.5	129	98	6.1	62.4	0.79	4.95E+05	0.3280	0.0593
VO-18D	392	163	141	98	5.8	62.4	0.77	7.28E+05	0.4390	0.0596
VO-18E	392	171	141	115	6.8	66.4	0.81	8.85E+05	0.5434	0.0595
VO-19A	366	107.5	109	83	2.4	47.6	0.75	3.66E+05	0.0694	0.0089
VO-19D	366	122.5	95	80	2.3	45.9	0.73	6.35E+05	0.1474	0.0064
VO-19E	366	131.5	118	73	3.0	49.6	0.75	5.53E+05	0.1786	0.0548
VO-21A	120	164.5	116	106	4.8	58.5	0.78	2.02E+05	0.1475	0.1407
VO-21C	120	145	125	115	4.9	59.9	0.79	3.18E+05	0.1541	0.0491
VO-21D	120	123.5	116	89	3.2	51.9	0.76	4.53E+05	0.1428	0.0466
VO-21E	120	134.5	116	96	3.7	54.2	0.77	6.38E+04	0.1243	0.0518

Sm	U	Th	Sm	eU	Th/U	Unc. Age	**C. Age**	Unc.	notes
ng	ppm	ppm	ppm	ppm	ppm/ppm	Ma	**Ma**		
0.4871	48	6	160	49	0.1	30.7	**40.4**	± 3	
0.6328	103	16	168	107	0.2	47.0	**60.2**	± 5	
0.5287	68	14	163	71	0.2	42.2	**57.8**	± 5	
0.9372	48	5	84	50	0.1	45.1	**55.7**	± 4	
0.8537	59	13	65	62	0.2	78.6	**94.7**	± 8	
0.4954	78	27	117	84	0.3	48.5	**64.6**	± 5	
0.6282	128	10	118	130	0.1	68.7	**89.2**	± 7	
0.5302	135	10	141	137	0.1	61.3	**79.6**	± 6	
0.5212	139	33	147	147	0.2	59.3	**78.0**	± 6	
0.8863	21	7	147	23	0.4	47.4	**58.5**	± 5	
0.6280	20	14	189	24	0.7	47.3	**60.6**	± 5	
0.9439	30	9	167	32	0.3	51.4	**64.2**	± 5	
0.5276	31	40	173	40	1.3	37.9	**51.2**	± 4	
0.6574	36	16	131	40	0.5	58.9	**74.5**	± 6	
0.4836	27	8	228	29	0.3	117.8	**166.0**	± 13	
0.4268	37	24	285	43	0.7	86.2	**126.8**	± 10	
0.6976	41	14	239	44	0.3	63.6	**88.3**	± 7	
0.3905	44	31	312	51	0.7	51.3	**64.2**	± 5	
0.4778	54	28	295	60	0.5	141.7	**208.5**	± 17	Inclusion?
0.5477	47	8	347	48	0.2	60.9	**84.6**	± 7	
0.0044	1	2	1	1	2.1	77.3	**97.9**	± 8	
0.6625	78	7	156	80	0.1	74.9	**98.6**	± 8	
0.6312	69	17	182	73	0.2	85.7	**114.2**	± 9	
1.0563	77	5	106	79	0.1	108.7	**132.6**	± 11	
0.6915	80	9	182	82	0.1	70.9	**94.5**	± 8	
0.8527	68	4	103	69	0.1	82.8	**102.2**	± 8	
0.5148	147	9	140	149	0.1	76.1	**104.2**	± 8	
0.4758	103	85	197	124	0.8	63.4	**90.6**	± 7	
0.3463	137	366	160	225	2.7	52.6	**75.9**	± 6	Th/U*
0.4391	206	12	199	209	0.1	71.4	**100.6**	± 8	
0.5245	103	35	155	112	0.3	78.6	**106.2**	± 8	
0.0665	2	3	13	3	1.3	46.6	**58.2**	± 5	
0.5543	26	14	150	29	0.5	59.2	**76.9**	± 6	
0.5158	40	35	154	48	0.9	53.9	**75.9**	± 6	
0.5916	25	26	112	31	1.0	58.5	**76.0**	± 6	
0.4020	5	1	17	5	0.1	60.5	**68.8**	± 6	
0.6241	46	40	174	56	0.9	67.8	**90.4**	± 7	
0.566	24	12	131	27	0.5	67.3	**88.5**	± 7	
0.6221	40	7	180	42	0.2	95.6	**130.9**	10	Inclusion?
0.5949	29	9	158	31	0.3	83.0	**112.1**	9	Inclusion?
0.5170	43	8	180	45	0.2	89.5	**119.3**	10	Inclusion?
0.2553	32	28	272	39	0.9	81.4	**131.3**	± 11	Inclusion?
0.4857	28	12	140	30	0.4	52.1	**70.4**	± 6	
0.7986	25	2	87	25	0.1	66.1	**82.6**	± 7	
0.4266	27	9	133	29	0.3	57.9	**79.3**	± 6	
0.9091	35	1	67	35	0.0	62.9	**76.7**	± 6	
0.4362	24	5	136	26	0.2	54.3	**74.4**	± 6	
0.5100	75	12	188	78	0.2	82.2	**114.1**	± 9	
0.6557	54	10	108	57	0.2	71.8	**90.9**	± 7	
0.5943	76	10	103	79	0.1	76.2	**98.9**	± 8	
0.7449	80	9	110	82	0.1	88.3	**109.0**	± 9	
0.4405	29	4	181	29	0.1	96.8	**129.1**	± 10	
0.5270	66	3	234	66	0.0	78.7	**107.8**	± 9	
0.6085	60	18	204	64	0.3	70.0	**93.3**	± 7	
0.6161	31	30	129	38	1.0	43.1	**55.3**	± 4	
0.6263	31	10	128	34	0.3	75.3	**95.3**	± 8	
0.5776	45	15	182	48	0.3	75.6	**99.5**	± 8	
0.5491	34	14	150	37	0.4	75.2	**97.6**	± 8	

MASSIF CENTRAL

Sample	El. (m)	ρ_d	n_d	ρ_s	n_s	ρ_i	n_i	n_g	$P(\chi^2)$ (%)	Central Age±1σ (Ma)	U (μg/g)	Lm±1σ (μm)	s.d. (μm)	n	Dpar (μm)	s.d.
vo-3	213	3.55	2086	14.7	1498	13.8	1400	20	1.6	**68.2±3.8**	46.1	13.6±0.2	1.7	101	1.8(94)	0.5
vo-4	323	3.53	2074	16.4	1154	13.0	914	20	19.9	**79.6±4.4**	43.4	12.8±0.2	1.7	78	2.5(87)	1.1
vo-14	1123	3.59	2112	20.0	1505	13.7	1033	20	80.2	**93.2±4.4**	45.0	13.9±0.1	1.5	100	1.9(117)	0.3
vo-16	461	3.50	2061	12.07	855	10.1	855	20	71.1	**75.0±4.0**	33.7	12.8±0.3	1.3	26	2.3(86)	0.6
vo-21	120	3.57	2099	16.5	1072	14.2	923	20	8.3	**74.4±4.5**	47.6	13.5±0.1	1.5	100	1.3(124)	0.3

Notes - Ages determined by external detector method using a zeta value for dosimeter CN5 ζ = 360 ± 11 (referred to Fish Canyon Tuff and Durango apatite standards, Hurford, 1990). El (m): sample elevations in metres; ρ_d, ρ_i: standard and induced track densities measured on mica external detectors; ρ_s: spontaneous track densities on internal mineral surfaces, track densities are given in 10^5 tracks cm^{-2}; n_d, n_i and n_s: number of tracks on external detectors and on mineral surfaces; n_g: number of counted mineral grains; $P(\chi^2)$: (χ^2) probability (Galbraith, 1981); Central age calculated using TRACKKEY program (Dunkl, 2002); Lm: mean length of confined tracks length distribution ± standard error, s.d.: standard deviation. Dpar: mean etch pit diameter parallel to the c-axis for age grains; Dpar: mean etch pit diameter parallel to the c-axis and number of total measured Dpar for sample; Samples were irradiated in the Lazy Susan facility of the Triga Mark II reactor of the LENA, University of Pavia (Italy).